MITSUBISHI ELECTRIC RESEARCH LABORATORIES
https://www.merl.com

On the Characteristics of One-Dimensional Compressible Flow

Qiao, Hongtao; Kobayashi, Takashi; Laughman, Christopher R.; Bortoff, Scott A.

TR2024-001 January 05, 2024

Abstract

Eigen decomposition of the governing equations that describe one-dimensional compressible flow has been presented. Analytical solution of the characteristics of the flow was derived. Simulation studies were conducted to support the theoretical analyses and wave propagation results were discussed in detail. It was found that acoustic effect introduced by the dynamic momentum led to a significant slowdown in the simulation and could be neglected in models without significant loss in accuracy for applications where energy transfer is of greater interest.

International Modelica Conference 2023

Mitsubishi Electric Research Laboratories, Inc.
201 Broadway, Cambridge, Massachusetts 02139

On the Characteristics of One-Dimensional Compressible Flow

Hongtao Qiao[1,*] Takashi Kobayashi[2] Christopher R. Laughman[1] Scott A. Bortoff[1]

[1]Mitsubishi Electric Research Laboratories, Cambridge, MA, USA,{qiao,laughman,bortoff}@merl.com

[2]Mitsubishi Electric Corporation, Hyogo 661-8661, Japan,
kobayashi.takashi@ds.mitsubishielectric.co.jp

Abstract

Eigen decomposition of the governing equations that describe one-dimensional compressible flow has been presented. Analytical solution of the characteristics of the flow was derived. Simulation studies were conducted to support the theoretical analyses and wave propagation results were discussed in detail. It was found that acoustic effect introduced by the dynamic momentum led to a significant slowdown in the simulation and could be neglected in models without significant loss in accuracy for applications where energy transfer is of greater interest.

Keywords: model reduction, characteristic speed, compressible flow, hyperbolic PDE, acoustic effect

1 Introduction

The equations that govern the motion of one-dimensional compressible flow are the system of hyperbolic partial differential equations (PDEs). These consist of conservation laws for mass, momentum, and energy. Acoustic waves appear in a compressible flow, and pressure perturbation involves perturbation of density, velocity, and other parameters. To capture the acoustic effect often requires very small integration steps when solving the governing equations, which significantly increases the computational cost. In contrast, energy transfer often involves a much slower time constant than other transport phenomena, and acoustic effect resulting from pressure perturbation is of minor importance. Consequently, many efforts have explored model reduction techniques to improve computational efficiency without significantly compromising model integrity.

One area of focus has been the simplification of the momentum equation since it usually does not affect the thermal system behavior over the time scales of interest in the applications where acoustic effect is not a top concern. Qiao and Laughman (2018) compared different model reduction techniques and showed that neglecting the phenomena on small time scales can improve numerical efficiency with a minimal loss in prediction accuracy based on simulation studies. However, the paper failed to present a theoretical proof to support their conclusions. Brasz and Koenig (1983) discussed the consequence of eliminating some terms in the original set of governing equations and found that the magnitude of the maximum characteristic speed was a key factor to limit the integration time step. Unfortunately, the authors did not provide detailed derivations to help readers fully understand the underlying reasoning. To fill in the gap, this paper will present a theoretical study for the propagation of waves in a fluid flowing through a channel, with an emphasis on applying the method of characteristics to solve the governing equations and elucidate the effect of dynamic momentum and acceleration pressure loss on the acoustic effect.

The remainder of the paper is organized as follows. In Section 2, we present detailed derivations for the eigen decomposition of governing equations for one-dimensional flow. In Section 3, we perform case studies to discuss the effect of dynamic momentum and acceleration pressure loss on the behavior of two-phase flow. Conclusions from this work are then summarized in Section 4.

2 Eigen Decomposition of Governing Equations

Without taking into account the gravitational force and axial heat conduction, the governing equations of mass, momentum and energy for one-dimensional flow with constant cross-sectional area can be written as

$$\frac{\partial \rho}{\partial t}+\frac{\partial G}{\partial x}=0 \tag{1}$$

$$\frac{\partial G}{\partial t}+\frac{\partial}{\partial x}\left(\frac{G^2}{\rho}\right)=-\frac{\partial p}{\partial x}-\frac{4\tau_w}{D_H} \tag{2}$$

$$\frac{\partial}{\partial t}(\rho e)+\frac{\partial}{\partial x}(Gh)=\frac{G}{\rho}\left(\frac{\partial p}{\partial x}+\frac{4\tau_w}{D_H}\right)+\frac{4q''}{D_H} \tag{3}$$

where ρ, G, p, e, h, τ_w, D_H and q'' are fluid density, mass flux, pressure, specific internal energy, specific enthalpy, wall shear stress, hydraulic diameter and heat flux, respectively.

δ_1 and δ_2 is introduced here to evaluate the impact of the dynamic momentum term $\frac{\partial G}{\partial t}$ and the acceleration pressure loss term $\frac{\partial}{\partial x}\left(\frac{G^2}{\rho}\right)$ on the transient characteristics of fluid flow. Multiplying G/ρ on both sides of Eq. (2) and substituting it into Eq. (3) yields

$$\delta_1 \frac{\partial G}{\partial t} + \delta_2 \frac{\partial}{\partial x}\left(\frac{G^2}{\rho}\right) = -\frac{\partial p}{\partial x} - \frac{4\tau_w}{D_H} \tag{4}$$

$$\frac{\partial}{\partial t}(\rho e) + \frac{\partial}{\partial x}(Gh) + \frac{G}{\rho}\left[\delta_1 \frac{\partial G}{\partial t} + \delta_2 \frac{\partial}{\partial x}\left(\frac{G^2}{\rho}\right)\right] = \frac{4q''}{D_H} \tag{5}$$

In general, pressure p, specific enthalpy h and mass flux G are selected as dynamic states in the simulation of vapor compressor cycles. Using the chain rule to expand $d\rho = \left(\frac{\partial \rho}{\partial p}\right)_h dp + \left(\frac{\partial \rho}{\partial h}\right)_p dh$, Eq. (1), (4) and (5) can be written in the quasilinear form after some manipulations

$$B(U)\frac{\partial U}{\partial t} + A(U)\frac{\partial U}{\partial x} = R \tag{6}$$

where

$$U = \begin{bmatrix} p \\ h \\ G \end{bmatrix},\ R = \frac{4}{D_H}\begin{bmatrix} 0 \\ -\tau_w \\ q'' \end{bmatrix},$$

$$B = \begin{bmatrix} \frac{\partial \rho}{\partial p} & \frac{\partial \rho}{\partial h} & 0 \\ 0 & 0 & \delta_1 \\ -1 & \rho & \delta_1 v \end{bmatrix},\ v = \frac{G}{\rho},$$

$$A = \begin{bmatrix} 0 & 0 & 1 \\ 1-\delta_2 v^2 \frac{\partial \rho}{\partial p} & -\delta_2 v^2 \frac{\partial \rho}{\partial h} & 2\delta_2 v \\ -\delta_2 v^3 \frac{\partial \rho}{\partial p} & G-\delta_2 v^3 \frac{\partial \rho}{\partial h} & 2\delta_2 v^2 \end{bmatrix}$$

It is evident that the conservation laws described by Eq. (6) are hyperbolic inhomogeneous PDEs. The characteristic speed of information propagation dx/dt can be found by solving the eigenvalue of $B^{-1}A$ via $|\lambda I - B^{-1}A| = 0$, where $|...|$ indicates the determinant and λ is the eigenvalue.

However, B is singular and does not have an inverse if the dynamic term in Eq. (4) is neglected, i.e., $\delta_1 = 0$. Note that A is always invertible regardless of the values of δ_1 and δ_2. Hence, Eq. (6) can be rewritten as

$$\frac{\partial U}{\partial x} + A^{-1}B\frac{\partial U}{\partial t} = A^{-1}R \tag{7}$$

Eq. (7) is also hyperbolic PDEs with characteristic speed dx/dt that is the reciprocal of the eigenvalue of $A^{-1}B$, i.e., $\left|\frac{dt}{dx}I - A^{-1}B\right| = 0$.

One can augment Eq. (6) with the total derivative of U

$$\begin{bmatrix} B & A \\ dtI & dxI \end{bmatrix}\begin{bmatrix} \frac{\partial U}{\partial t} \\ \frac{\partial U}{\partial x} \end{bmatrix} = \begin{bmatrix} R \\ dU \end{bmatrix} \tag{8}$$

where I is a 3×3 identity matrix.

It is shown below that the characteristic speeds of the system described by Eq. (6), dx/dt, are actually the roots of the determinant of the coefficient matrix of Eq. (8), regardless of whether B is singular or not.

$$\begin{aligned} 0 &= \begin{cases} \left|\frac{dx}{dt}I - B^{-1}A\right| & \text{for } |B| \neq 0 \\ \left|\frac{dt}{dx}I - A^{-1}B\right| & \text{for } |B| = 0 \end{cases} \\ \Rightarrow 0 &= \begin{cases} (dt)^3\left|\frac{dx}{dt}I - B^{-1}A\right||B| & \text{for } |B| \neq 0 \\ -(dx)^3\left|\frac{dt}{dx}I - A^{-1}B\right||A| & \text{for } |B| = 0 \end{cases} \\ \Rightarrow \Delta &= \begin{vmatrix} B & A \\ dtI & dxI \end{vmatrix} = \left|\frac{dx}{dt}B - A\right|(dt)^3 = 0 \end{aligned} \tag{9}$$

With both dynamic momentum term and acceleration pressure loss term included in Eq. (6), i.e., $\delta_1 = \delta_2 = 1$, the determinant of the coefficient matrix is given by

$$\Delta = \frac{\rho}{c^2}\left(\frac{dx}{dt} - v\right)\left[c^2 - \left(\frac{dx}{dt} - v\right)^2\right](dt)^3 = 0 \tag{10}$$

where $c = \sqrt{1/\left(\frac{\partial \rho}{\partial p} + \frac{1}{\rho}\frac{\partial \rho}{\partial h}\right)}$. It is evident that there are three distinct characteristics for the system

$$\frac{dx}{dt} = v - c, v, v + c \tag{11}$$

Next, we show that c is the speed of sound. Since the change in density can be determined as $d\rho = \left(\frac{\partial \rho}{\partial p}\right)_h dp + \left(\frac{\partial \rho}{\partial h}\right)_p dh$, one can have

$$\left(\frac{\partial \rho}{\partial p}\right)_s = \left(\frac{\partial \rho}{\partial p}\right)_h + \left(\frac{\partial \rho}{\partial h}\right)_p \left(\frac{\partial h}{\partial p}\right)_s \tag{12}$$

Using the relation $dh = Tds + \frac{1}{\rho}dp$, one can obtain

$$\left(\frac{\partial h}{\partial p}\right)_s = \frac{1}{\rho} \tag{13}$$

Substituting Eq. (13) into Eq. (12) yields

$$c = \sqrt{\frac{1}{\left(\frac{\partial \rho}{\partial p}\right)_h + \frac{1}{\rho}\left(\frac{\partial \rho}{\partial h}\right)_p}} = \sqrt{\left(\frac{\partial p}{\partial \rho}\right)_s} \tag{14}$$

The right-hand side of Eq. (14) is the definition of the speed of sound.

We use the symbols {−, ◦, +} to denote these three eigenvalues of $B^{-1}A$, i.e., v - c, v, v + c. The corresponding eigenvectors are

$$r^{(-)} = -\frac{2c}{\rho}\begin{bmatrix} c^2 \\ \frac{\partial h}{\partial \rho} + c^2 \frac{\partial h}{\partial p} \\ v - c \end{bmatrix}, r^{(\circ)} = \frac{1}{T\frac{\partial \rho}{\partial h}}\begin{bmatrix} 0 \\ \frac{\partial h}{\partial \rho} \\ v \end{bmatrix},$$
$$r^{(+)} = \frac{2c}{\rho}\begin{bmatrix} c^2 \\ \frac{\partial h}{\partial \rho} + c^2 \frac{\partial h}{\partial p} \\ v + c \end{bmatrix} \tag{15}$$

where the coefficients are carefully chosen so that the characteristic variables introduced below can be in a simple form.

Letting matrix Q be the matrix of eigenvectors, i.e., $Q = \left(r^{(-)}|r^{(\circ)}|r^{(+)}\right)$, $B^{-1}A$ can be diagonalized as

$$Q^{-1}B^{-1}AQ = \begin{bmatrix} v - c & 0 & 0 \\ 0 & v & 0 \\ 0 & 0 & v + c \end{bmatrix} = \Lambda \tag{16}$$

Defining the characteristic variables W as $dW = Q^{-1}dU$, we can write Eq. (7) as

$$\frac{\partial W}{\partial t} + \Lambda \frac{\partial W}{\partial x} = Q^{-1}B^{-1}R \tag{17}$$

Eq. (17) is equivalent to Eq. (18) - (20).

$$dW^{(-)} = dv - \frac{dp}{\rho c} = -\frac{4}{\rho D_H}\left(\frac{q''}{c}\frac{1}{\rho\frac{\partial h}{\partial p}\Big|_\rho - 1} + \tau_w\right)dt$$
$$\text{for } \frac{dx}{dt} = \lambda^{(-)} = v - c \tag{18}$$
$$dW^{(\circ)} = ds = -\frac{4q''}{c^2 D_H T\frac{\partial \rho}{\partial h}}\frac{1}{\rho\frac{\partial h}{\partial p}\Big|_\rho - 1}dt$$
$$\text{for } \frac{dx}{dt} = \lambda^{(\circ)} = v \tag{19}$$
$$dW^{(+)} = dv + \frac{dp}{\rho c} = \frac{4}{\rho D_H}\left(\frac{q''}{c}\frac{1}{\rho\frac{\partial h}{\partial p}\Big|_\rho - 1} - \tau_w\right)dt$$
$$\text{for } \frac{dx}{dt} = \lambda^{(+)} = v + c \tag{20}$$

Eq. (19) denotes that entropy wave $W^{(\circ)} = s$ travels with local flow speed of v, whereas Eq. (18) and (20) denote that backward acoustic wave $W^{(-)} = v - \int \frac{dp}{\rho c}$ and forward acoustic wave $W^{(+)} = v + \int \frac{dp}{\rho c}$ travel with sonic speed of c with respect of local flow speed v, as shown in Fig. 1. When the flow is adiabatic and inviscid (R = 0), Eq. (6) becomes Euler equations and three waves will remain constant along their respective characteristic curve (Doyle, 2006). However, this is nonphysical and cannot occur in the real world. For fluid flow with heat transfer, the variations in the entropy are only determined by the heat flux along $dx = vdt$. Positive heat flux results in an increase in entropy and negative heat flux results in a decrease in entropy. For viscous flow, frictional losses always lead to the attenuation of both acoustic waves, as shown in Eq. (18) and (20). Meanwhile, Eq. (18) and (20) indicate that heat flux imposes opposite impact on two acoustic waves, because positive heat flux in the forward

direction is equivalent to negative heat flux in the backward direction.

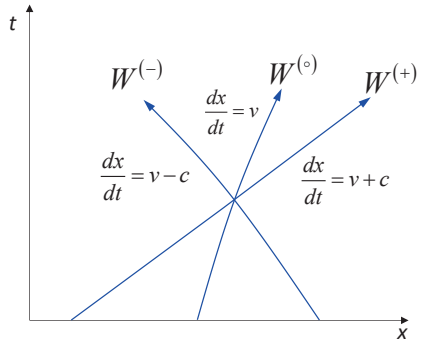

Figure 1. Characteristics of the original set of governing equations

Following the above analyses, one can compute the characteristic speeds of the system when acceleration pressure loss is neglected, i.e., $\delta_1 = 1$, $\delta_2 = 0$.

$$\Delta = \frac{\rho}{c^2}\left(\frac{dx}{dt}-v\right)\left[c^2-\left(\frac{dx}{dt}\right)^2\right](dt)^3 = 0 \qquad (21)$$

It is evident that there are also three distinct characteristic speeds, i.e., $\frac{dx}{dt} = -c, v, c$. These three characteristics correspond to three waves, i.e., backward acoustic wave $W^{(-)} = -\int \frac{dp}{\rho c}$, entropy wave $W^{(\circ)} = s$ and forward acoustic wave $W^{(+)} = \int \frac{dp}{\rho c}$. Again, two acoustic waves travel with sonic speed c.

When dynamic momentum is neglected, i.e., $\delta_1 = 0$, $\delta_2 = 1$, the determinant of the coefficient matrix becomes

$$\Delta = \frac{\rho}{c^2}\left(\frac{dx}{dt}-v\right)\left(v^2-c^2-2v\frac{dx}{dt}\right)(dt)^3 = 0 \qquad (22)$$

Only two distinct characteristic speeds exist in this case, $\frac{dx}{dt} = \frac{v^2-c^2}{2v}, v$, corresponding to a supersonic backward acoustic wave and a forward entropy wave.

If neither dynamic momentum term nor acceleration pressure loss term is considered, i.e., $\delta_1 = \delta_2 = 0$, the determinant of the coefficient matrix is

$$\Delta = \rho\left(\frac{dx}{dt}-v\right)(dt)^3 = 0 \qquad (23)$$

In this case, the acoustic effect is eliminated and there is only one characteristic speed $\frac{dx}{dt} = v$, corresponding to the entropy wave travelling along with flow.

CFL stability condition must hold if the FTUS (Forward in Time, Upwind in Space) scheme is employed to solve Eq. (6).

$$\frac{|\lambda|_{\max}\Delta t}{\Delta x} \le C_{\max} = 1 \qquad (24)$$

where Δt is the time step, Δx is the length interval, and λ is the eigenvalue of the flux Jacobian ($B^{-1}A$) with the largest absolute value (or the reciprocal of the eigenvalue of $A^{-1}B$ with the smallest absolute value). It is evident from Eq. (24) that the time step is restricted by the fastest characteristic speed. When either dynamic momentum term or acceleration pressure loss is taken into consideration, time steps need to be extremely small to obtain a stable solution since the fastest characteristic speed contains the speed of sound. In comparison, when neither term is included, much larger time steps can be taken since the CFL condition becomes $\frac{v\Delta t}{\Delta x} \le 1$. In this case, v is the only characteristic speed, and it is often much smaller than the speed of sound c.

3 Results and Discussions

The finite volume method is often used to discretize the governing equations that describe the dynamics of fluid flow because it has been highly successful in approximating the solution of a wide range of thermal-fluid systems and maintaining quantity conservation. In many of these types of models, a staggered grid scheme is utilized to decouple the mass and energy balance equations from the momentum balance equation. As a result, the mass and energy balances are calculated within the volume cells while the momentum balance is calculated within the flow cells, as depicted in Fig. 2.

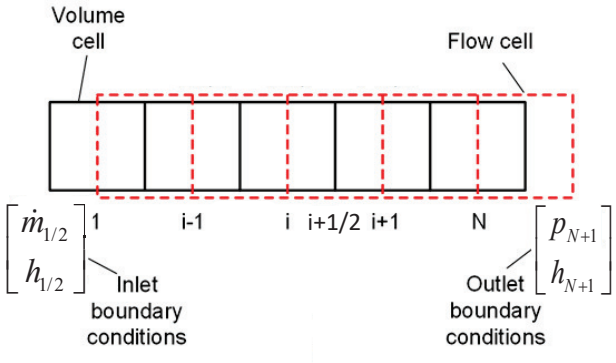

Figure 2. Staggered grid scheme

To simplify the analysis, homogeneous equilibrium model (HEM), which assumes liquid and vapor phases are in thermodynamic equilibrium and have the same phasic velocities, was used to calculate thermodynamic

properties of two-phase. As a result, Eq. (6) can be discretized as (Qiao et al., 2015)

$$\frac{\partial \rho_i}{\partial p_i}\frac{dp_i}{dt}+\frac{\partial \rho_i}{\partial p_i}\frac{dh_i}{dt}=\frac{G_{i-1/2}-G_{i+1/2}}{\Delta x_i} \tag{25}$$

$$\delta_1\frac{dG_{i+1/2}}{dt}+\delta_2\frac{\dot{I}_{i+1}-\dot{I}_i}{A\Delta x_i}=-\frac{p_{i+1}-p_i}{\Delta x_i}-\frac{4\tau_{w,i+1/2}}{D_H} \tag{26}$$

$$\rho_i\frac{dh_i}{dt}-\frac{dp_i}{dt}+v_{i+1/2}\left(\delta_1\frac{dG_{i+1/2}}{dt}+\delta_2\frac{\dot{I}_{i+1}-\dot{I}_i}{A\Delta x_i}\right) =\frac{G_{i-1/2}\left(h_{i-1/2}-h_i\right)-G_{i+1/2}\left(h_{i+1/2}-h_i\right)}{\Delta x_i}+\frac{4q_i''}{D_H} \tag{27}$$

Based on the above discretized form, a dynamic model for one-dimensional channel flow was created in Modelica with inlet boundary conditions defined as mass flow rate and specific enthalpy and outlet boundary conditions as pressure and specific enthalpy, as depicted in Fig. 3. Please note that specific enthalpy at the outlet was only useful when reverse flow occurred.

Four case studies were conducted, and each case corresponded to a combination of δ_1 and δ_2 with different values, i.e., Case 1 ($\delta_1 = 1$, $\delta_2 = 1$), Case 2 ($\delta_1 = 1$, $\delta_2 = 0$), Case 3 ($\delta_1 = 0$, $\delta_2 = 1$) and Case 4 ($\delta_1 = 0$, $\delta_2 = 0$). The flow was assumed to be adiabatic so that the effect of heat transfer on wave propagation can be precluded. For Case 1 and 2, the flow was assumed to be inviscid ($\tau_w = 0$) since pressure could be decoupled from mass flux by the dynamic momentum. For Case 3 and 4, however, frictional pressure loss between adjacent segments needed to be considered since pressure and mass flux were coupled through algebraic relations. Frictional pressure loss was approximated as follow (Laughman and Qiao, 2018)

$$\Delta p=\Delta p_0\left(\dot{m}/\dot{m}_0\right)^2 \tag{28}$$

To perform a fair comparison between these cases, frictional pressure loss in the Case 3 and 4 needed to be very small. Δp_0 and $\dot{m}_0$ were chosen to be 5 Pa and 0.005 kg/s, respectively.

The flow channel was 6m long with hydraulic diameter of 0.01m and was divided into 50 segments with equal size. R-32 was the working fluid, and its properties were computed based on the patch-based B-spline approach (Laughman and Qiao, 2021). The mass flow rate and specific enthalpy at the source was 0.005 kg/s and 380 kJ/kg, respectively. The pressure and specific enthalpy of the sink was fixed at 820 kPa and 382 kJ/kg, respectively. For all cases, models were initialized with steady-state condition and subject to a step change in the specific enthalpy of the source at t = 0, from 382 kJ/kg to 458 kJ/kg. Simulations were carried out in the Dymola 2023x environment (Dassault Systemes, 2023). With the Euler solver, smaller time steps ($\Delta t < 4e\text{-}7s$) were required to yield stable solutions for Case 1 and 2. For Case 3 and 4, much larger time steps could be used ($\Delta t < 2e\text{-}5s$). The results shown below were obtained with the DASSL solver with a tolerance of 1e-6.

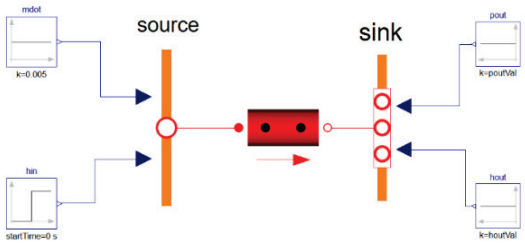

Figure 3. Modelica model of channel flow with a step change in inlet enthalpy

Fig. 4 illustrated the profiles of pressures along the flow channel at various time instants for Case 1. At t = 0, pressures were uniform everywhere. With a sudden increase in specific enthalpy at the inlet, two-phase flow with higher vapor quality entered the channel, resulting in an increase in pressure due to more vapor accumulating in the first segment. This high-pressure wave (it is related to the term of $\int\frac{dp}{\rho c}$ in $W^{(-)}$ and $W^{(+)}$) would travel forward with a speed of $v+c$ along the flow channel, as show in Fig. 4a. At 0.032 sec, the front of the pressure wave reached the exit of the channel and the average wave speed was around 187 m/s, which was very close to the value of $v + c$. The pressure in last segment could not vary freely since the pressure boundary at the exit was fixed. At 0.04 sec, the pressure in the last segment increased to its maximum. Due to the enlarged pressure difference between the last segment and the channel exit, more flow left the channel and pressure in the last segment started to decline. Accordingly, the upstream pressures would be affected, and pressure wave would bounce back. The reflection behavior was similar to the reflection of any waves with fixed end. It was interesting to notice that the wave front kept its shape after reflection. As shown in Fig. 4b, at 0.046 sec the pressure in the last segment reached to its minimum and corresponded to a peak of outflow. At around 0.08 sec, the backward wave reached the inlet of the channel and its average speed was about -176 m/s, which was very close to the value of $v - c$. Since the outflow of the first segment exceeded its inflow at this point, the pressure would decrease accordingly. Based on the behavior of wave reflection with free end, the pressure of the first segment could decrease to a much lower value than the equilibrium pressure, resulting in an inverted low-pressure wave. At 0.088 sec, the

pressure of the first segment reached its minimum and then pressure wave traveled forward again (Fig. 4c). At 0.12 sec, the low-pressure wave reached the channel exit again and reflects with a similar shape. At 0.16 sec, the backward pressure wave reached the inlet of the channel once more (Fig. 4d). Then the pressure in the first segment would elevate quickly, and a high-pressure wave with the same phase as the initial forward wave built up and thus finished up a complete cycle.

Fig. 5 showed the profiles of mass flow rates along the flow channel for Case 1. At t = 0, mass flow rate was equal to 5 g/s everywhere. As the pressures near the inlet of the channel started to build up, resulting in negative pressure gradients. From Eq. (26), it was easy to deduce that negative pressure gradients tend to accelerate the flow. Therefore, a mass flow wave (it is related to the term of v in $W^{(-)}$ and $W^{(+)}$) that corresponded to the pressure wave formed and propagated forward. At 0.034 sec, mass flow wave reached the exit of the channel (Fig. 5a). At the same time, the reflecting backward pressure wave retained its negative slope at the wave front, resulting in further acceleration of the flow. Because the mass flow rate was not fixed at the exit, it was amplified by twice of the magnitude of the mass flow wave at 0.0445 sec (Fig. 5b). Similarly, the mass flow wave was inverted at the free end and traveled back towards the inlet of the channel. At 0.08 sec, the high mass flow wave reached the inlet. Since the inverted forward pressure wave resulted in positive pressure gradients at the wave front, the fluid flow started to decelerate. The reflected mass flow wave kept its shape since it was fixed at the inlet and reached the exit once again at 0.12 sec (Fig. 5c). At the exit, the corresponding pressure wave reflected with unchanged positive slopes at wave front, leading to further deceleration of the flow. Consequently, the mass flow rate at the exit declined by more than twice of the magnitude of the wave at 0.13 sec. As the inverted low mass flow wave traveled backwards, mass flow rates behind the wave front oscillated around the equilibrium (Fig. 5d). At 0.16 sec, the wave reached the inlet of the channel. As the corresponding high-pressure wave started to form at this point, the mass flow wave finished a complete cycle.

Fig. 6 depicted the profiles of entropies along the flow channel for Case 1. Initially, the entropy of the flow was 1147 J/(kg·K) everywhere. As a result of a sudden increase in specific enthalpy at the inlet, the entropy in the first segment increased rapidly. It can be observed that entropy wave traveled along with the flow and the wave front flattened out with time. At around 4 sec, entropy profile reached a new equilibrium. Different from pressure wave and mass flow wave, entropy wave traveled along with the flow at a much slower speed and did not bounce back at the boundaries, which corroborated the derivations in the previous section.

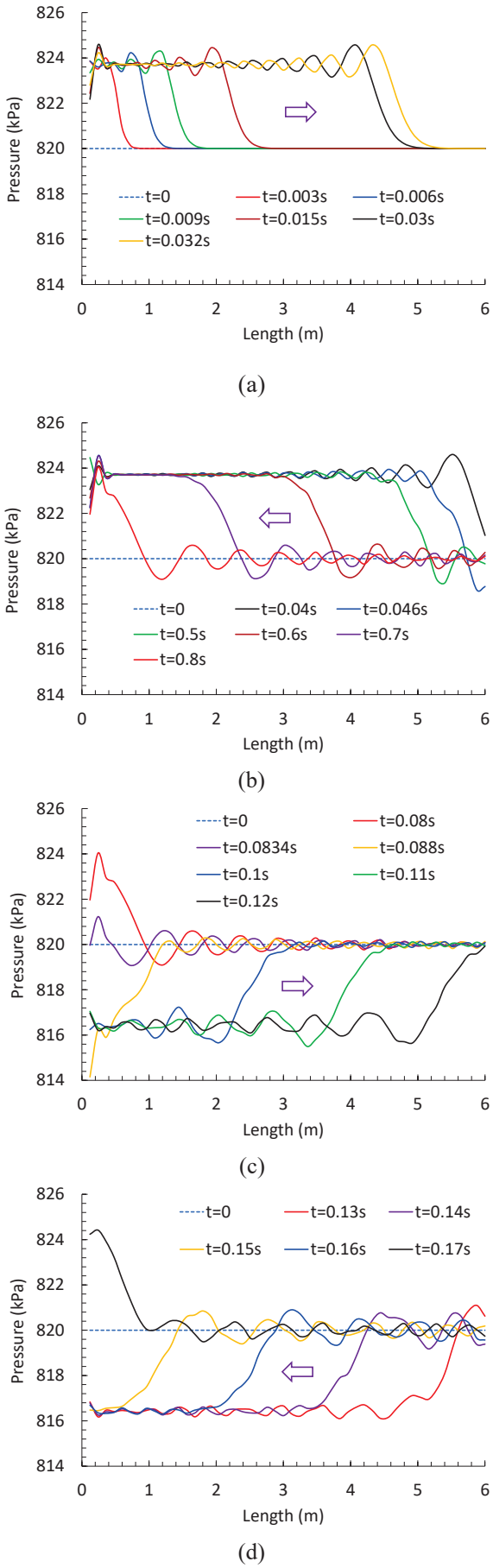

Figure 4. Pressure profiles along flow channel (Case 1)

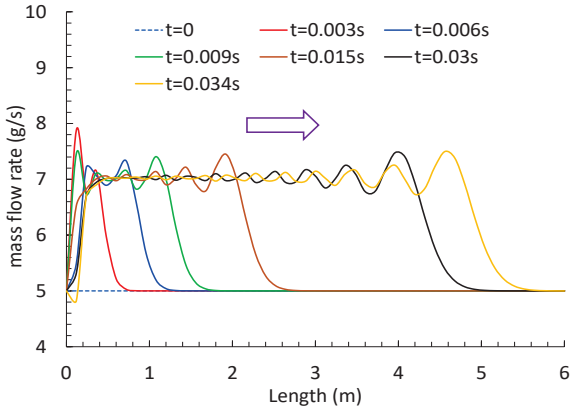

(a)

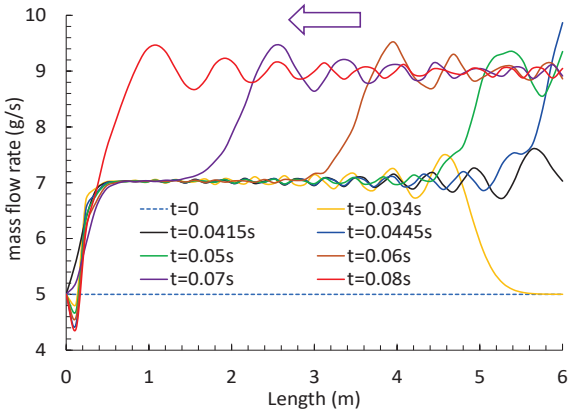

(b)

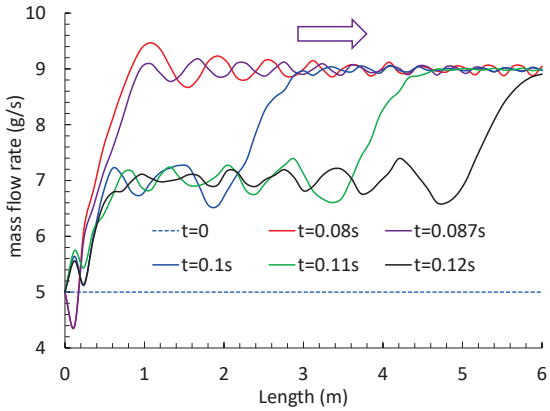

(c)

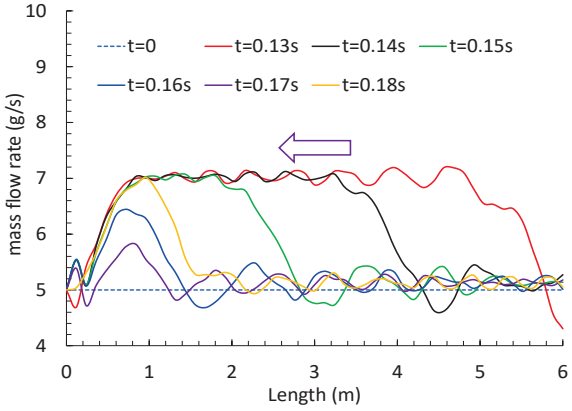

(d)

Figure 5. Flow profiles along flow channel (Case 1)

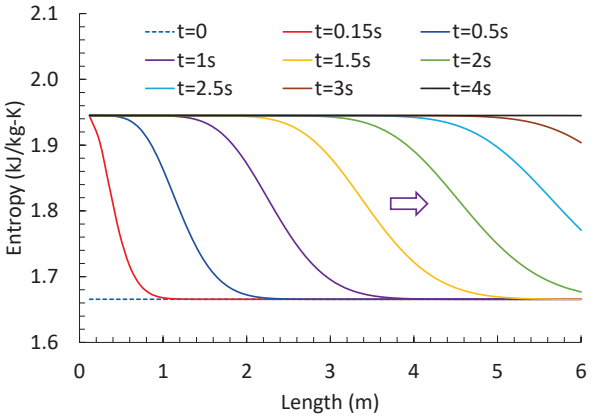

Figure 6. Entropy profiles along flow channel (Case 1)

The profiles of pressures, mass flow rates and entropies along the flow channel for Case 2 were plotted in Fig. 7 to 9. As discussed in the previous section, merely neglecting the acceleration pressure loss did not lead to major changes in the characteristics of the flow except that the speeds of acoustic waves changed slightly. Hence, the interpretation of the results in Case 2 will be the same as in Case 1.

Fig. 10 to 12 displayed the profiles of pressures, mass flow rates and entropies along the flow for Case 3. Although two analytical characteristics existed, i.e., $\frac{v^2-c^2}{2v}, v$, the backward supersonic wave was not physical and did not show up in the results. Like the entropy wave, the mass flow wave did not exhibit any acoustic effect. At 3.5 sec, the wave died out and mass flow rates were back to their equilibrium condition. Due to the frictional pressure loss, the equilibrium pressure profile was not flat. Since the dynamic term was neglected, the speed of pressure propagation should be infinite. Overall, pressure variations were well-behaved, and the rippling effect at the beginning dissipated very quickly.

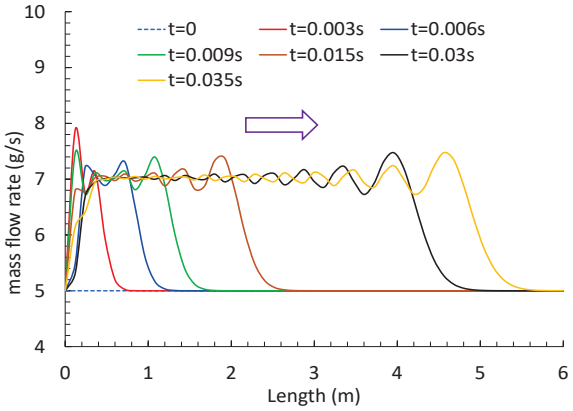

(a)

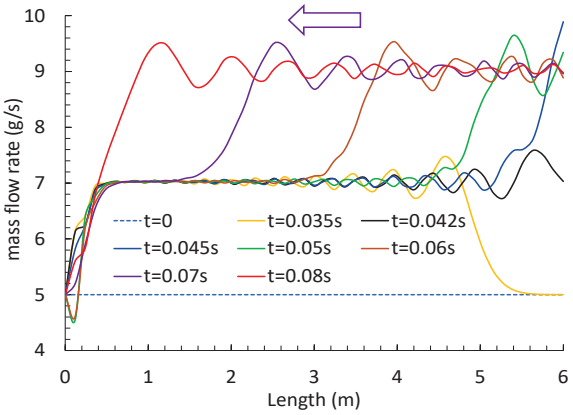

(b)

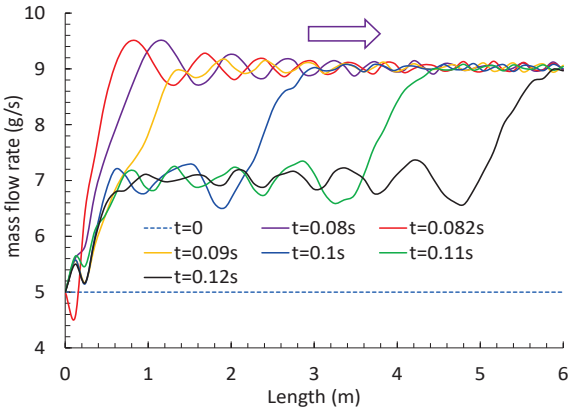

(c)

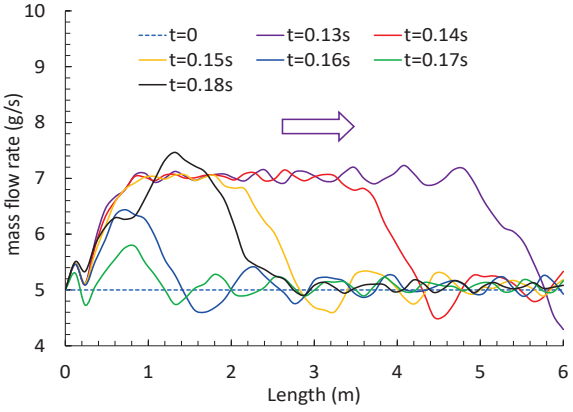

(d)

Figure 7. Flow profiles along flow channel (Case 2)

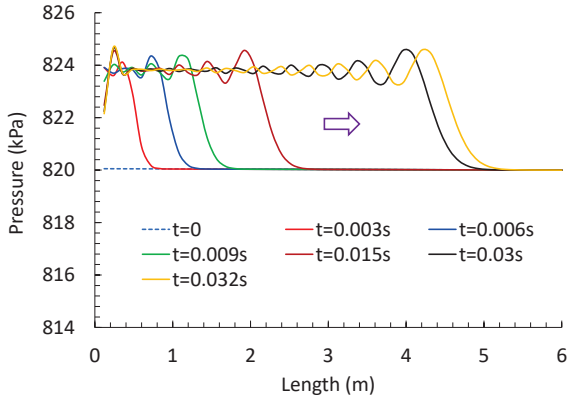

(a)

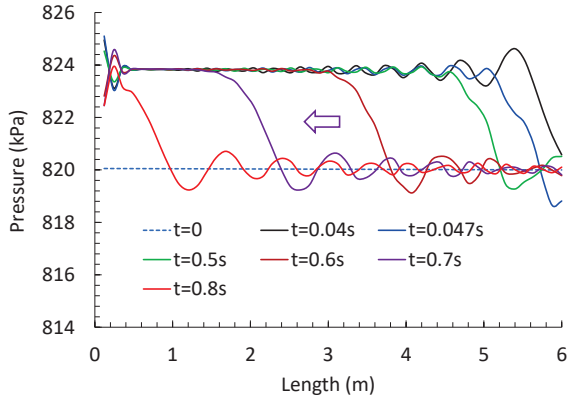

(b)

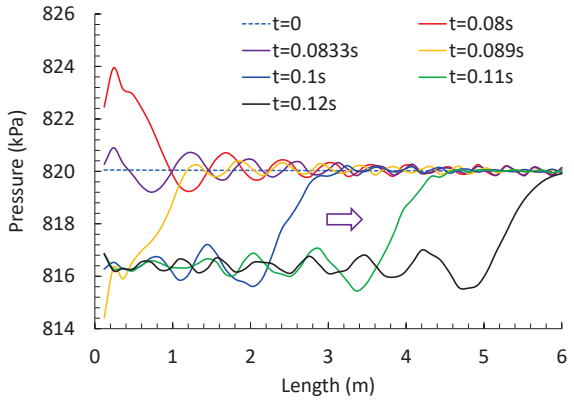

(c)

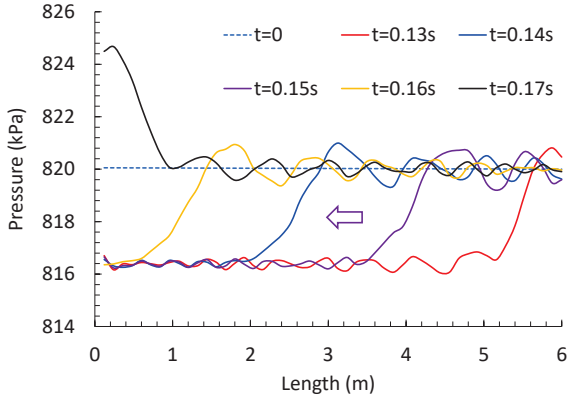

(d)

Figure 8. Pressure profiles along flow channel (Case 2)

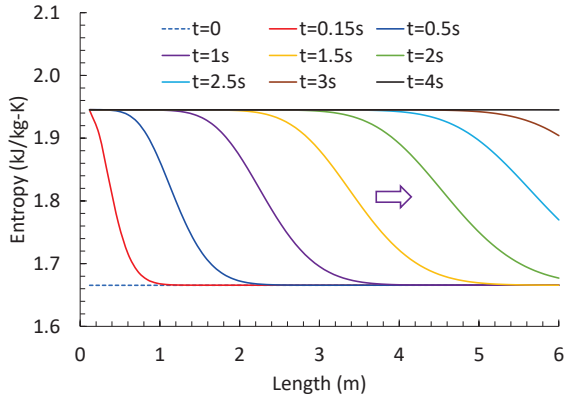

Figure 9. Entropy profiles along flow channel (Case 2)

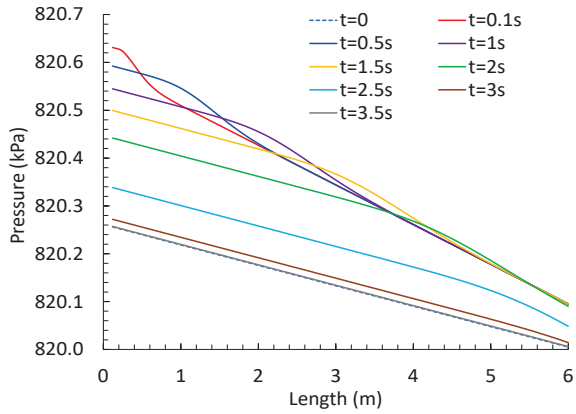

Figure 10. Pressure profiles along flow channel (Case 3)

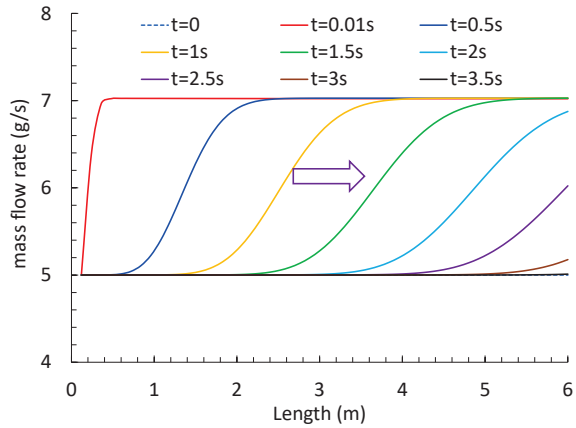

Figure 11. Flow profiles along flow channel (Case 3)

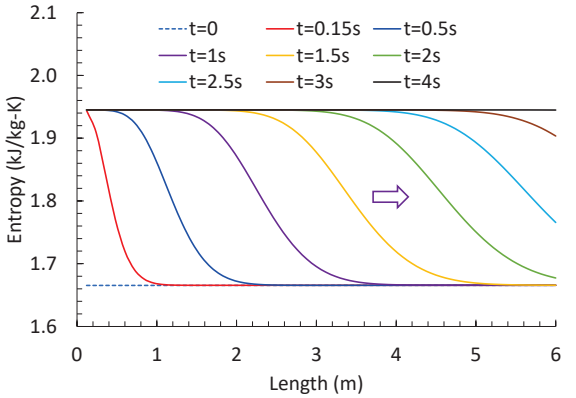

Figure 12. Entropy profiles along flow channel (Case 3)

The profiles of pressures, mass flow rates and entropies along the flow channel at various time instants for Case 4 were manifested in Fig. 13 to 15. This was the simplest case with only one characteristic speed. Again, entropy wave and mass flow wave traveled along with the fluid and did not reflect at the boundaries. Compared with Case 3, no rippling effect was observed in the pressure profiles.

Comparison of simulation speed between these cases indicates that Case 1 was the slowest, followed by Case 2 and then Case 3, while Case 4 was the fastest. For 15 sec simulation, CPU time of these cases was 240 sec, 180 sec, 7 sec and 1 sec, respectively. At the end of simulation, acoustic wave effect was still in place for both Case 1 and Case 2, whereas in Case 3 and 4 steady-state conditions arrived at around t = 4 sec. Profiling showed that pressures and mass flows were the dominating states for Case 1 and 2, whereas pressures and specific enthalpies were the dominating states for Case 3 and 4.

Solver choice did not exhibit noticeable effect on the results as long as the solutions were stable, but the computational speeds could vary significantly. With the Euler solver, the simulation speeds were substantially slower than the DASSL solver. In comparison, the CPU time for these cases were 42894 sec, 21215 sec, 649 sec, and 604 sec, respectively. This indicated that the BDF methods were much more numerically efficient than the explicit fixed time step methods.

The above analysis indicated that both dynamic momentum term and acceleration pressure loss term imposed significant impact over simulation speed and accuracy. In the applications where acoustic effect is not a great concern, these terms can be neglected in models to achieve much higher computational performance at the expense of accuracy.

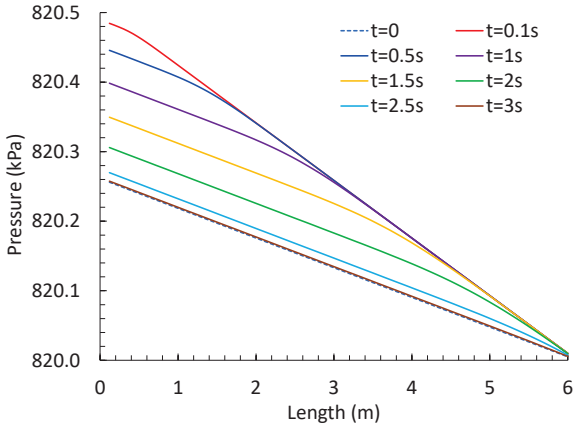

Figure 13. Pressure profiles along flow channel (Case 4)

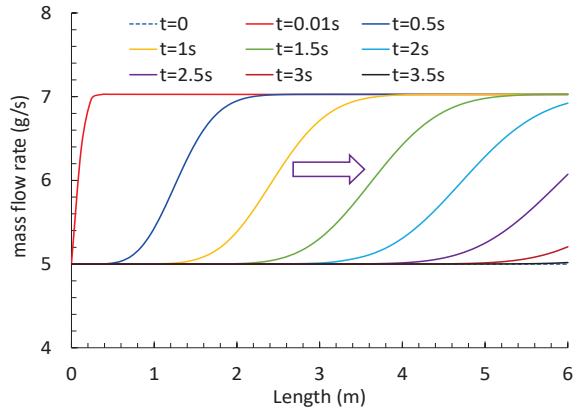

Figure 14. Flow profiles along flow channel (Case 4)

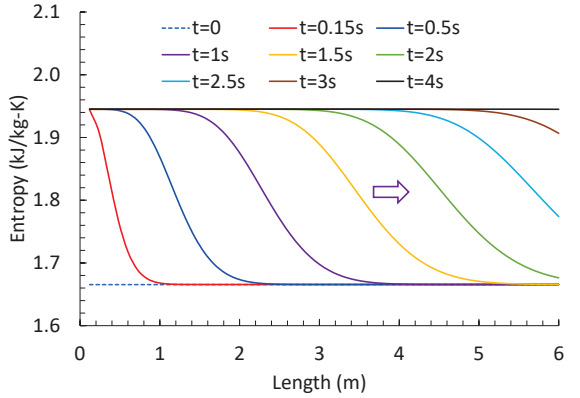

Figure 15. Entropy profiles along flow channel (Case 4)

4 Conclusions

This paper explored the effect of dynamic momentum and acceleration pressure loss on the characteristics of one-dimensional compressible flow. Eigen decomposition for the governing equations was shown to obtain their characteristic form and analytical solution for the wave speeds was derived. Simulation studies were performed to provide evidence to the theoretical analyses. It was found that acoustic effect arising from the dynamic momentum greatly affected the simulation speed. Meanwhile, it was shown that both dynamic momentum and acceleration pressure loss may be neglected in models to speed up simulations in applications where energy transfer is more important than momentum transfer.

References

Christopher Laughman and Hongtao Qiao. On closure relations for dynamic vapor compression cycle models. American Modelica Conference, 2018.

Christopher Laughman and Hongtao Qiao. Patch-based thermodynamic property models in the subcritical region. 18th International Refrigeration and Air Conditioning Conference at Purdue, 2021.

Dassault Systemes, AB. Dymola 2023x, 2023.

Hongtao Qiao and Christopher Laughman. Comparison of approximate momentum equations in dynamic models of vapor compression systems. In Proceedings of the 16th International Heat Transfer Conference, 2018.

Hongtao Qiao, Vikrant Aute and Reinhard Radermacher. Transient modeling of a flash tank vapor injection Heat Pump System - Part I: Model Development. *International Journal of Refrigeration*, No. 49, pp. 169–182, 2015.

Joost Brasz and Kenneth Koenig. Numerical methods for the transient behavior of two-phase flow heat transfer in evaporators and condensers. *Numerical Properties and Methodologies in Heat Transfer*, pp: 461-476, 1983.

Knight Doyle. Elements of Numerical Methods for Compressible Flows. Cambridge Aerospace Series, Cambridge: Cambridge University Press, 2006.